



Impacts of climate change on terrestrial hydrological components and crop water use in the Chesapeake Bay watershed

Parthkumar A. Modi, Daniel R. Fuka, Zachary M. Easton*

Department of Biological Systems Engineering, Virginia Tech, Blacksburg, VA, 24061, USA

ARTICLE INFO

Keywords:

Noah-MP
Crop water use
MACA
Global climate models
Climate change

ABSTRACT

This study assessed the impacts of climate change on terrestrial hydrological components and Crop Water Use (CW_U) over the Chesapeake Bay watershed using a combination of Global Climate Models (GCMs) and a land surface model. To better understand the impacts of climate change on the hydrological cycle, long-term simulations of multiple earth system models from the Coupled Model Intercomparison Project (CMIP Phase 5) are statistically downscaled and bias-corrected using Multivariate Adaptive Constructed Analogs (MACA) scheme for use as model forcing. Precipitation indices from the twenty MACA-based GCMs are used to identify six best performing models. A mesoscale approach is developed, where CW_U is estimated by accounting for the impacts of changing climate conditions and rising CO_2 levels. Daily grid-based crop coefficients are derived from evapotranspiration data. The findings indicate a significant annual increase in precipitation (10 %) and temperature (+4.5 K) for the RCP 8.5 scenario towards the end of the 21st century. A significant reduction (13 % and 17 % respectively) in CW_U is estimated for corn and soybeans, resulting from increased total precipitation and rising CO_2 levels suppressing evapotranspiration. Our results indicate that even in a warmer regime, crop water use decreased due to rising CO_2 concentrations due to climate change.

1. Introduction

Increases in global CO_2 emissions have led to significant changes in climatic conditions (Solomon et al., 2009). These changes, often manifested in the precipitation and temperature, have and will continue to affect regional water availability (Solomon et al., 2007; Wagena et al., 2016) and crop production (Brown et al., 2015). Climate change has direct impacts on crop growth due to changes in temperature, water availability, or CO_2 concentrations, and indirect impacts due to the more rapid changes in weed, insect, and pathogen pressures associated with these climatic changes (Varanasi et al., 2016). Each of these pressures can affect crop water use. Increasing temperatures intensify the water cycle making more water available in the atmosphere for storms but contributing to increased evapotranspiration, and increasing atmospheric CO_2 concentrations can suppress crop water use (Deryng et al., 2016; Urban et al., 2017). In the U.S., climate change is expected to cause a northward shift in storm tracks, resulting in increases in the North and East US (Baldini et al., 2016). However, these changes vary by season and depend on regional weather patterns such as El Niño and La Niña.

Climate projections for the Chesapeake Bay watershed suggest an increase in annual precipitation with more significant precipitation in the winter and spring and less in the summer and fall (Najjar et al., 2010; Pyke et al., 2008; Rosenzweig et al., 2004; Wagena

* Corresponding author at: 303 Seitz Hall, Virginia Tech, 155 Ag Quad Lane, Blacksburg, VA, 24061, USA.

E-mail address: zeaston@vt.edu (Z.M. Easton).

et al., 2018) and projected warming of 2–6 °C throughout the 21 st century (Hayhoe et al., 2007; Najjar et al., 2010). These changes in precipitation and temperature interact to affect crop growth in complex ways (Brown et al., 2015; Hayhoe et al., 2007; Pyke et al., 2008). For instance, changes in crop growth may be least impacted under scenarios of moderate warming without significant shifts in the timing or magnitude of precipitation but result in reduced growth if dry periods coincide with times when crops are most sensitive to water shortages (Elliott et al., 2014). In addition to changing weather patterns, atmospheric CO₂ concentrations play a crucial role in crop water use. Increased atmospheric CO₂ levels can increase agricultural productivity by enhancing photosynthesis rates while suppressing leaf-level transpiration, ultimately reducing plant water use (Kimball and Idso, 1983; Vanuytrecht, 2012). However, the interactions between changes in precipitation, temperature, atmospheric CO₂ concentrations, and plant/vadose zone processes make inferring the impact of climate change on plant water use difficult.

Crop Water Use (CW_U) is the metric often used to quantify the amount of water used to achieve optimal crop growth for estimating gross plant requirements (Döll and Siebert, 2002). In many regions, CW_U is estimated using crop models (Elliott et al., 2014; Konzmann et al., 2013), which represent the dynamics between the atmosphere, crop, and soil, ultimately simulating crop growth and development, water uptake, and transpiration (Holzworth et al., 2018). While crop models are powerful tools to predict crop phenology and water use, they are limited by their representation of the landscape where crops are grown, and in how they model water and nutrient transport (Stöckle and Kemanian, 2020).

Land surface models (LSMs), due to their coupled water and energy balance approach, can be used to simultaneously project future water availability (Hurkmans et al., 2008) and estimate the CW_U through simple crop management formulations (Döll and Siebert, 2002; Fischer et al., 2007; Yang et al., 2019), though the current limitations of included field-scale geospatial data included in the current Chesapeake Bay watershed model inhibits including the most recently published phenological level crop dynamics into this and other regional CW_U models, limiting these CW_U models benefits on future local and regional water availability (Koehler, 2020); in effect limiting our understanding of future food and environmental security.

We propose a simple mesoscale approach that incorporates parameterization from high-resolution topography and soil datasets to quantify the impacts of changing climatic conditions on future water availability and crop water use by accounting for increasing CO₂ levels. This study uses a soil water balance approach (evapotranspiration, soil moisture) and atmospheric CO₂ concentrations to estimate crop water use using a combination of GCMs and land surface model (Noah-MP) over rainfed and irrigated croplands in the Chesapeake Bay watershed. Six best performing GCM's are included based on the precipitation indices and two future scenarios (RCP

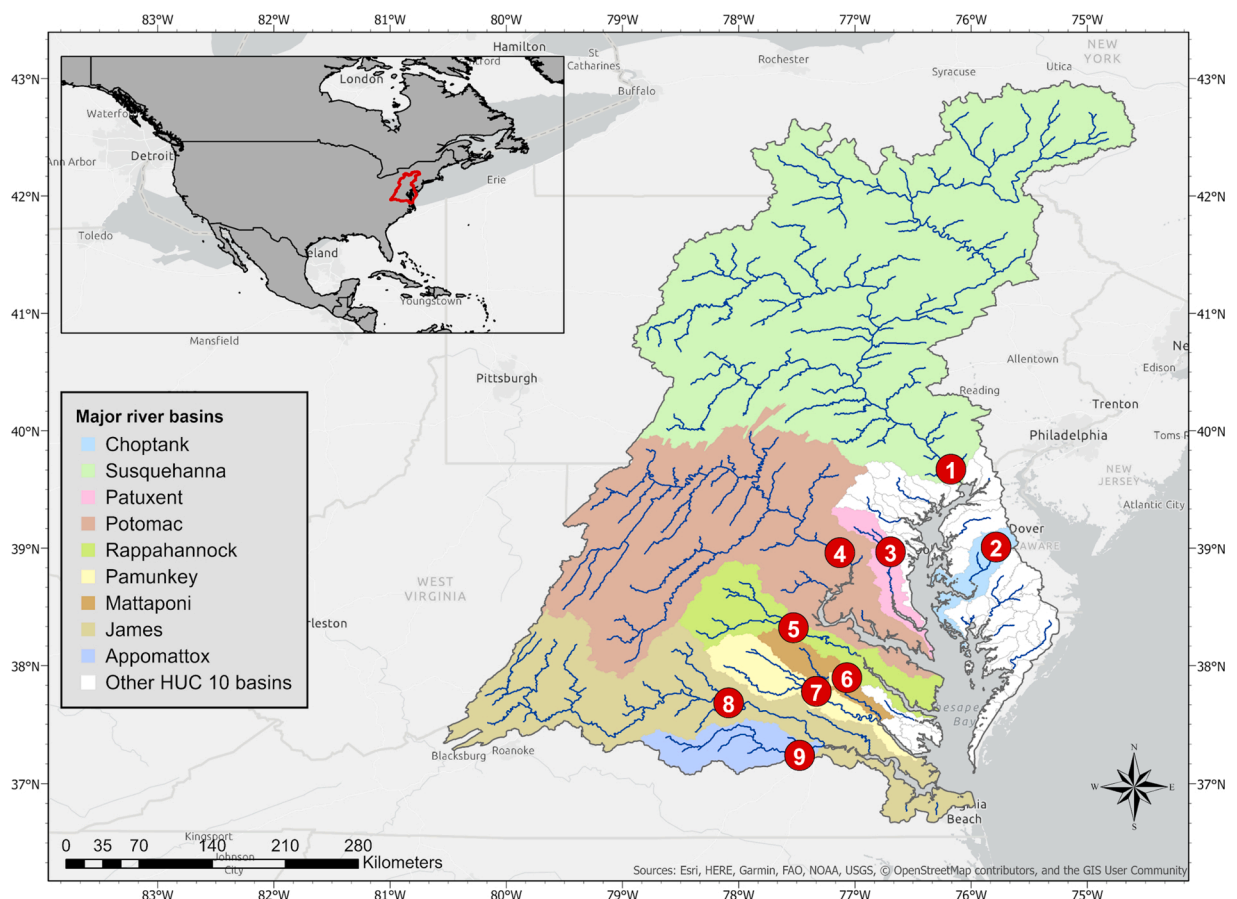


Fig. 1. Chesapeake Bay watershed with red circles indicating the hydrologic USGS streamgages as indicated in Table S1.

4.5 and RCP 8.5) are considered. The crop coefficients for different crops are estimated using available global evapotranspiration datasets which can be easily applied to a region without prior knowledge of its characteristics and at required spatiotemporal resolution. The objectives of this study are to understand the changes in water availability using climate projections and quantify the alteration in crop water use under the impact of climate change.

2. Study area

The Chesapeake Bay watershed occupies 165,760 km² with more than 18 million people residing in the watershed. Five major rivers form the Chesapeake Bay watershed; Susquehanna, Potomac, Rappahannock, York, and James. More than 100,000 streams, creeks, and rivers drain the Chesapeake Bay watershed with boundaries extending from headwaters of Otsego Lake, near Cooperstown, New York to Suffolk, Virginia, and outlet at Atlantic. The climate of the region is temperate-humid ([Chesapeake Bay Program, 2017](#)). As per the Chesapeake Bay watershed model (Phase 5.3.2 developed by CBP), 23 % of the land is used for agriculture, 6.4 % is the developed land, and 69.8 % forest. Water use is a major issue that must be evaluated with the increasing extent and intensity of the agricultural activities in the watershed and the ongoing effects of climate change. [Fig. 1](#) shows the Chesapeake Bay watershed and the USGS gage locations used for this study. The Chesapeake Bay watershed is divided into nine sub-basins corresponding to USGS gages located on the major tributaries (Table S1).

3. Data and methods

3.1. Noah-MP model and configuration

The Noah-MP land surface model, with the multi-parameterization scheme, is an improved version of the baseline Noah land surface model ([Ek et al., 2003](#); [Niu et al., 2011](#)). Noah-MP has an interactive vegetation canopy layer to compute canopy and ground surface temperatures with an embedded dynamic vegetation model. The choice of multi-parameterization includes several vegetation models (with an option of dynamic vegetation), radiation transfer, runoff, and groundwater schemes. The soil moisture content and its transition from wet to dry periods are largely affected by the runoff mechanism. The runoff schemes in Noah-MP include the infiltration excess - free drainage runoff ([Schaake et al., 1996](#)), a saturation excess based TOPMODEL runoff with an equilibrium water table [([Niu et al., 2005](#)); SIMTOP] and a simple TOPMODEL with groundwater model [([Niu et al., 2007](#)); SIMGM]. In SIMTOP, subsurface runoff is represented as an exponential function of water table depth by using a single coefficient to calculate the maximum subsurface runoff volume. The saturated hydraulic conductivity decreases with the soil depth and reduces uncertainty in the total runoff preventing the direct alteration of hydraulic conductivity, which dramatically affects other terrestrial hydrological components like evapotranspiration and soil moisture [([Niu et al., 2005](#)); SIMTOP]. The parameterization options used in this study are shown in Table S2.

Streamflow routing is performed using a stand-alone routing model ([Lohmann et al., 1996](#)), based on a unit-hydrograph method that uses daily surface runoff and baseflow to estimate the streamflow at gauge locations. To do this, flow direction and flow accumulation are determined to develop the routing network and then a convolution-based model, based on the unit hydrograph representing the travel time distribution, is used to route the streamflow at the USGS gaging stations. The digital elevation model (DEM) is hydrologically conditioned, and available at 3-sec spatial resolution, from the USGS Hydrosheds database ([Lehner et al., 2008](#)).

3.2. Model input data

Datasets needed to parameterize the model include surface albedo from the Moderate Resolution Imaging Spectrometer (MODIS), the green fraction from MODIS, landuse/landcover from United States Department of Agriculture – National Agricultural Statistics Service ([USDA, 2008](#)), leaf area index from MODIS, maximum snow albedo, soil type from State Soil Geographic (STATSGO), and soil temperature from WRF Preprocessing System (WPS) data page managed by UCAR ([UCAR/NCAR, 2020](#)). These datasets are used to configure the Noah-MP HRLDAS (High-Resolution Land Data Assimilation System) model and are assumed to be constant in time. The meteorological variables that are used to force Noah-MP include precipitation, mean temperature, specific humidity at 2 m, wind speed components at 10 m, downward longwave and shortwave radiation, and surface pressure. The model is set up at a 4 km spatial resolution with the input data forced at a daily time step.

3.3. Weather data

3.3.1. Historical reference/training dataset

The METDATA/gridMET dataset [([Abatzoglou, 2013](#)); gridded meteorological daily dataset] is available over the entire domain of conterminous United States (CONUS) and is a high-resolution gridded meteorological dataset available at 1/24-degree spatial resolution from 1979 to 2010. ([Abatzoglou, 2013](#)) developed METDATA by combining the temporally rich data from the North American Land Data Assimilation System Phase 2 (NLDAS 2) ([Mitchell, 2004](#); [Xia et al., 2012](#)) and spatially rich data from the Parameter-elevation Regressions on Independent Slopes Model [PRISM; ([Daly et al., 2008](#))]. One of the limitations of METDATA is that the source datasets (NLDAS and PRISM) do not account for evaporative cooling effects from agriculture, which implies that METDATA derived potential evapotranspiration (ET₀) estimates have systematic bias inherited from its source ([Abatzoglou, 2013](#); [Huntington et al., 2016](#)). Calibration parameters for Noah-MP particular to Chesapeake Bay watershed are estimated by comparing the output from

Noah-MP (forced by METDATA from 1980 to 2010) with several observed and remotely sensed products, described in section 3.5.

3.3.2. Bias correction and statistical downscaling

To force Noah-MP and incorporate the impacts of climate change, we use climate models from the MACAv2-METDATA version [now known as MACA-M; (Abatzoglou and Brown, 2012)] which is statistically downscaled and bias-corrected with METDATA as a training dataset for the entire CONUS using the constructed analogs (CA) method. (Glötter et al., 2014) concluded that current dynamical downscaling methods do not provide improved predictions over statistically bias-corrected GCM projections and MACAv2-METDATA contains all the inputs to Noah-MP including precipitation, minimum and maximum temperature, solar radiation, specific humidity, and wind speed components. The CA method is developed to match the patterns between the synoptic-scale field of Global Climate Models (GCM) and the set of observation patterns (Hidalgo et al., 2008). In simple terms, weather patterns today or in the future correspond to or exactly replicates the weather pattern following the time of the exact analog in the historical record (van den Dool, 2003; Van Den Dool, 1994). MACA (Multivariate Adaptive Constructed Analogs) uses the same approach except that it uses a multivariate analog search to improve coherence across downscaled fields. The GCM data are bias-corrected using the quantile mapping approach by spatially interpolating the data to the downscaled grid (Maurer et al., 2010). The epoch adjustment is used to avoid no analogs situations under future climate scenarios by removing the differences between the mean of future time slices and historical time slices on a 21-day moving window and adding or multiplying to the respective downscaled fields. Analogs were constructed from GCM's by identifying the 30 best predictor patterns as a single field or linear combinations that are matched with a library of observed patterns from METDATA falling within 45 days of the target date. Finally, epoch adjustment and bias correction are again performed to ensure statistical moments between historical observations and GCM's historical predictions are preserved.

The MACA dataset consists of 20 different GCM's from the Coupled Model Intercomparison Project 5 [CMIP5; (Taylor et al., 2012)] that includes data from historical (1950–2005) and two future Representative Concentration Pathways (RCPs): 4.5 (increase in radiation by 4.5 W/m^2 by 2100), and 8.5 (increase in radiation by 8.5 W/m^2 by 2100) from 2006 to 2100. For this study, two RCPs, 4.5 and 8.5 are selected, representing an intermediate baseline, and high-emission baseline scenario, respectively, where each GCM includes historical data (1976–2005) and two future periods, 2021–2050 (near future) and 2061–2090 (distant future) for each RCP scenario.

3.4. Selection of GCM's

To select representative GCMs, a series of indices are calculated that compare historical GCM predictions against the METDATA. Precipitation indices including the Annual Maximum Precipitation (AMP), Mean Annual Precipitation (MAP), frequency of precipitation (P-FREQ), and heavy to non-heavy precipitation ratio (H-NH) are calculated for both the statistically downscaled GCMs and the METDATA (Mishra et al., 2014). AMP for each year is the highest magnitude event for each year during the reference period of 1981–2005. P-FREQ is estimated as the number of precipitation events above the 99th percentile during the reference period, whereas H-NH is estimated by calculating the ratio of total precipitation due to heavy events ($> 99^{\text{th}}$ percentile) and total precipitation due to non-heavy events ($> 1 \text{ mm}$) during the reference period. The top six performing models are selected for use in this study. The six best performing models are identified by ranking each model within each index from least to most biased followed by the sum of ranks. The six models selected include CanESM2, CCSM4, CNRM-CM5, CSIRO-Mk3–6-0, HadGEM2-ES365, and IPSL-CM5A-LR. However, it should be noted that adequate model hindcast performance does not ensure reliable future predictions, but it is considered to be the only way to assign model confidence (Reichler and Kim, 2008).

Three out of the six GCM's (CCSM4, CSIRO-Mk3–6-0, IPSL-CM5A-LR) chosen are similar to the work of (Maloney et al., 2014) and (Sheffield et al., 2013) that ranked and analyzed the GCMs based on the bias with the observed precipitation and air temperature and which was later adapted by (Wagena and Easton, 2018) to study the impacts of climate change on agricultural conservation practices in Susquehanna River Basin in Chesapeake Bay watershed. There is no significant difference observed between the spatial plots of precipitation indices like AMP and MAP as the statistical moments of GCM's are preserved during the downscaling and bias correction. Extreme statistics related to precipitation indices like P-FREQ and H-NH are usually not preserved by bias correction (Hagemann et al., 2011) and they show a significant difference in the spatial patterns among the different GCM's when compared to METDATA. The spatial plot indicating the relative bias for different precipitation indices with respect to METDATA for six best performing GCMs is shown in Fig. S1. The evaluation of temperature is excluded from the selection of GCMs as they have a narrow range of uncertainty among the models with all of them showing a consistent, increasing trend in future climate scenarios.

3.5. Calibration and evaluation of Noah-MP

Noah-MP is calibrated for the water balance components including streamflow, evapotranspiration, and soil moisture. Monthly streamflow is calibrated for each of the nine stations (Table S1) in CBW with the USGS streamflow measurements from 1995 to 2001 and evaluated from 2002 to 2008 to ensure good model performance. Two evaluation metrics are used, the Nash Sutcliffe Efficiency (NSE) and the coefficient of determination (R^2). The NSE at each gaging station depends on the input forcing data, static model data, and model parametrization. The Theil-Sen slope estimator is used to estimate the trend and slope in the future periods relative to the baseline scenario. This non-parametric technique determines the median slope among the lines generated through pairs of two-dimensional sample points and computes trends insensitive to the outliers (Sen, 1968; Theil, 1950). The model was calibrated and run on the Computational Information Systems Laboratory supercomputing facilities at UCAR/NCAR. Noah-MP (forced by METDATA) is calibrated and evaluated using observed and derived products. A manual sub-basin calibration is performed using a combination of

literature values and expert judgment for the nine sub-basins as described in Table S3. Some parameters are distributed throughout the study domain and their calibration is performed on the basis of multiplier values rather than replacing the actual parameter values. The topographic mean in the SIMTOP runoff routine affects the partitioning of total excess moisture into surface runoff and baseflow and varies for each sub-basin. Noah-MP by default has a single value for topographic index throughout the domain but by manually configuring an additional layer of the topographic index into setup file and code, the topographic index mean for each sub-basin is used. The topographic index mean is further calibrated for each sub-basin based on the water balance components. Streamflow is calibrated by adjusting the runoff decay factor (FFF), baseflow coefficient (RSBMX), topographic index (TIMEAN), saturated hydraulic conductivity (DKSAT), and maximum soil moisture level (SMCMAX). ET is calibrated by adjusting the vegetation parameters including stomatal resistance (RS) and soil parameters including pore size distribution index (BEXP). For ET, model predictions are compared to the remotely sensed USGS SSEBop dataset from 2002 to 2008 (Senay et al., 2013). SSEBop method is based on the Simplified Surface Energy balance model that estimates ET using predefined boundary conditions between hot and cold reference values for each grid. SCAN [Soil Climate Analysis Network; (Schaefer et al., 2007)] station data led by the United States Department of Agriculture (USDA)/National Resources Conservation Service (NRCS) are used for calibrating the soil moisture of the top 10 cm layer. Five stations throughout the CBW are used to evaluate model performance from 2002 to 2008 using the coefficient of determination (R^2) and Root Mean Squared Error (RMSE). Soil moisture is calibrated using a combination of calibration parameters of ET and streamflow that includes the maximum soil moisture (SMCMAX) and pore size distribution index (BEXP).

3.6. Crop types and growing seasons

In this study, the USDA 2018 cropland data layer (CDL) with a 30 m spatial resolution is used. The classes from CDL are reassigned to the MODIS Noah International Biosphere-Geosphere Programme (IGBP) scheme [21 classes; (Strahler et al., 1999)] by grouping them as agricultural or non-agricultural classes. The CB watershed has two dominant crop types (corn and soybeans) which are predominantly located on the Delmarva Peninsula (East coast of Maryland, Delaware, and Virginia) and in York and Lancaster County in Pennsylvania. As per the statistics from USDA, the CB watershed contains 1.25 million hectares of corn and 0.78 million hectares of soybeans. The CDL is resampled to the model's spatial resolution using a maximum likelihood method of 30 m pixels in each 4 km grid cell. At 4 km model resolution, the maximum agricultural area derived is approximately 55 % for both corn and soybeans of the actual USDA acreage. The decrease in the crop acreage is because the 4 km grid cells in Noah-MP landcover are aggregated based on the neighboring algorithm. CW_U is strongly dependent on overall cropping pattern and climate conditions and hence it is not greatly affected by the decrease in crop acreage. This decrease in crop acreage can be resolved by increasing the model resolution, subject to the availability of the meteorological data at a higher spatial resolution.

Based on the USDA-NASS (2010), the typical planting and harvesting dates are obtained for both corn and soybeans (Table S4). From the estimated daily crop coefficients (as described in section 3.7) and the planting and harvesting dates, the initial crop growth stage, the crop development stage, the mid growth stage, and the harvest period are defined for both crops. The dates were in a similar range for all the states for both corn and soybeans, which allowed us to develop a single crop coefficient curve for each crop over the entire CB watershed. A fixed growth duration is considered for both the crops instead of the varying growth duration calculated using GDD (Growing Degree Days). The varying growth duration is driven by both climatic changes as well as technological advancement in agronomics, which necessitates the use of crop models to generate various scenarios based on historical records of management practices. Past studies have reported either a decrease in the crop growing length (He et al., 2015; Zhang et al., 2013) or little to no change in crop growing duration due to change in cultivars (Liu et al., 2012, 2009; Sacks and Kucharik, 2011). Considering either of the univariate scenarios (in case of varying growth duration) to derive the change in growing duration length might mislead the estimates of CW_U .

3.7. Current and future crop water use (CW_U)

Crop water use, CW_U (mm/day), is determined using a soil water balance approach [Eq. 1] (National Engineering Handbook, 1993). Effective rainfall, P_E , [Eq. 2] is the difference between gross water inputs via precipitation (P) and irrigation (In_C) and loss of rootzone available moisture via runoff and interflow (TR). P_E represents the amount of moisture stored in the crop root zone that can be used for crop evapotranspiration. Since our interest is in times of water deficit, i.e., soil below saturation, we limit this analysis to crop root zone and therefore only consider the effect of total runoff and not deep percolation in estimating effective rainfall.

$$CW_U = P_E - ET_C \quad (1)$$

$$\text{where } P_E = P + In_C - TR \quad (2)$$

$$ET_C = ET_o * K_C * B_C * C_D \quad (3)$$

Where P_E is the effective rainfall (mm/day), ET_C is the actual crop evapotranspiration (mm/day) computed using Eq. 3, ET_o is the potential evapotranspiration (mm/day), K_C is the 10-day mean daily crop coefficient, B_C is the monthly bias correction factor, P is the total precipitation (mm/day), TR is the total runoff including surface runoff and baseflow (mm/day), C_D is the carbon dioxide (CO_2) correction factor. P_E is estimated using the water fluxes from the Noah-MP land surface model that includes inputs (precipitation and irrigation) and losses (surface runoff, interflow, and baseflow). ET_o for future periods is calculated from the energy fluxes of Noah-MP

using the Penman-Monteith formulation with inputs as mean air temperature, wind speed, relative humidity, and net radiation from GCMs.

Daily crop coefficients, K_C , are by definition defined as the ratio of actual ET to potential ET [used in Eq. 3]. Thus, we determined K_C as the ratio of USGS SSEBop actual ET to NOAA global reference potential evapotranspiration (ET_0). The historic ET_0 estimations from NOAA are based on Global Data Assimilation System (GDAS) drivers from Senay et al. (2008), who used ASCE's standard Penman-Monteith formulation to derive ET_0 estimates using Modern-Era Retrospective Analysis for Research and Application (MERRA2) Reanalysis product. The ratio is estimated from 2000 to 2017 and is averaged over the years (2000–2017) to get a daily crop coefficient. To reduce the uncertainty due to precipitation variability, a 10-day moving mean is used. The use of historically validated datasets ensures that the calculation of crop coefficient accounts for soil water stress and crop growth under natural conditions.

We estimate monthly bias correction factors, B_C , and a CO_2 correction factor [used in Eq. 3] to account for bias from GCMs and impacts of CO_2 emissions on crop evapotranspiration, C_D , respectively. Monthly bias correction factors are calculated by taking the ratio of METDATA derived ET_0 estimates (from Noah-MP) and NOAA reference evapotranspiration from 2000 to 2017, multiplied by projections from GCM's ET_0 estimates (Huntington et al., 2016). To account for the effects of rising CO_2 concentrations, stomatal conductance functions developed by Kruijt et al. (2008) for C_3 and C_4 crops are used to estimate CO_2 correction factors for each crop (C_D). These factors account for the impacts of rising CO_2 concentrations on stomatal aperture, transpiration, and crop growth and are calculated using Eq. 4 (Huntington et al., 2016):

$$C_D = (1 - (S_{gs} * S_T * \Delta CO_2)) \quad (4)$$

$$S_{gs} = (dg_s/g_s)/dCO_2 \quad (5)$$

$$S_T = (dT/T)/(dg_s/g_s) \quad (6)$$

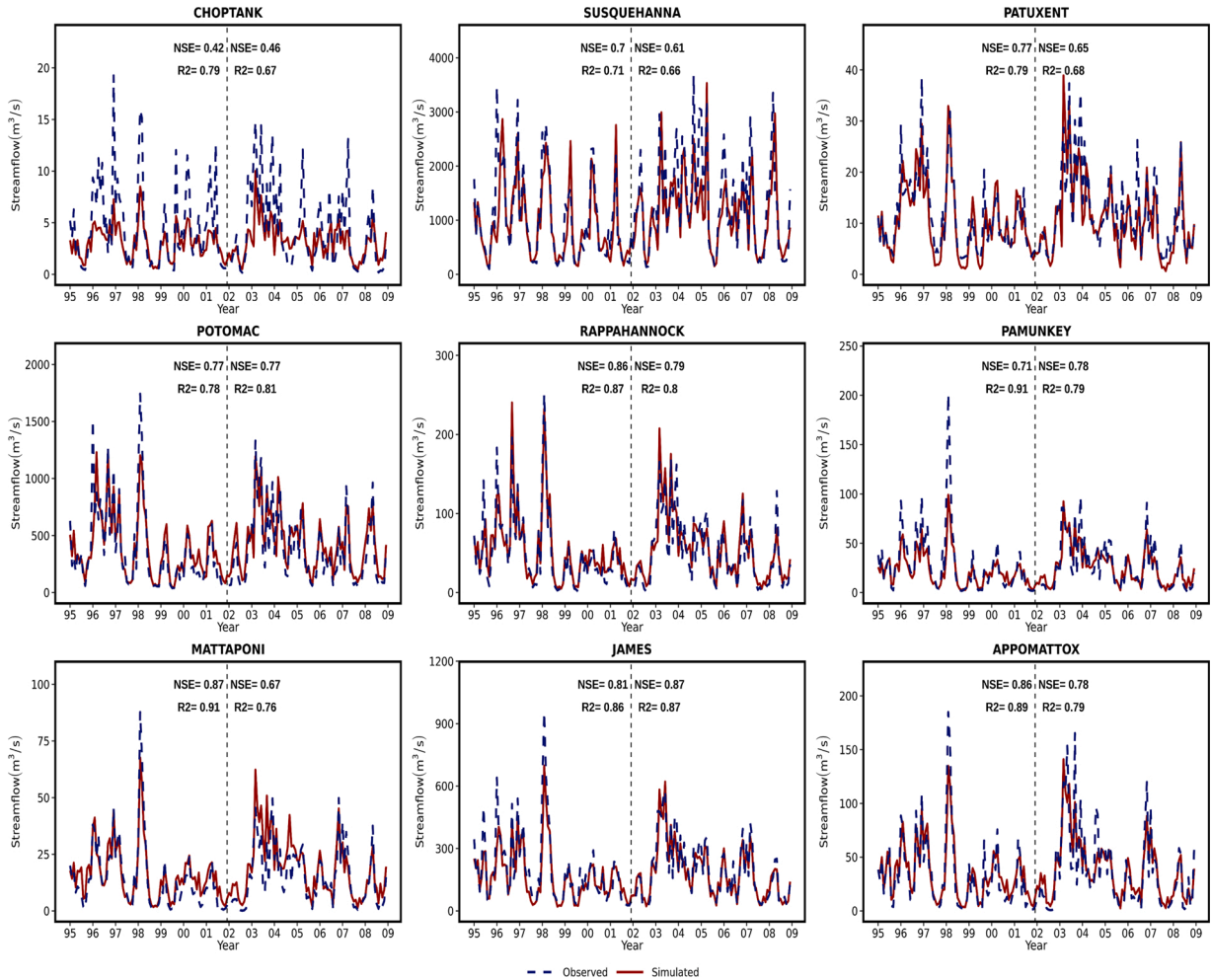


Fig. 2. Monthly calibration (left to the dotted line; 1995–2001) and evaluation (right to the dotted line; 2002–2008) of streamflow with USGS streamflow gage data for nine stations in Table S1. Note the different scales for Y-axis (streamflow).

Where C_D is the CO_2 correction factor, ΔCO_2 is the change in CO_2 concentration (ppm) relative to a historical baseline, S_{gs} is the relative sensitivity of crop stomatal conductance (g_s) to CO_2 (ppm^{-1}) computed using Eq. 5, and S_T is the relative sensitivity of transpiration (T in $kg\ m^2\ s^{-1}$) to a change in crop stomatal conductance (dimensionless) computed using Eq. 6, with sensitivities derived from Jacobs and Bruin (1997,1992) & Kruijt et al. (2008). As suggested by Huntington et al. (2016), the CO_2 correction factors (C_D) for the respective C_3 (soybeans) and C_4 (corn) crops are calculated at daily time steps for both RCP 4.5 and RCP 8.5.

4. Results and discussion

4.1. Model performance evaluation

Fig. 2 shows the monthly calibration (left; 1995–2001) and evaluation (right; 2002–2008) of streamflow for the Noah-MP model. All stations except Choptank had NSE values and R^2 greater than 0.6 for both calibration and evaluation periods signifying good model performance over the entire CB watershed. The Choptank is dominated by groundwater flow due to the presence of shallow unconfined aquifers and short groundwater recharging paths (Sun et al., 2017). The streamflow was highly sensitive to the partitioning of input precipitation and soil parameters such as saturated hydraulic conductivity. The SIMTOP runoff scheme used in this study is governed by the topographic index of the respective sub-basin, runoff decay factors, and the baseflow coefficient, which differ substantially between the majority of the basin and the coastal plain Choptank.

The difference between the model predicted ET and actual ET from the USGS indicated an underestimation of 10–15 % in the Coastal plain region and overprediction of 40 % in the urban areas, which can be attributed to a simple urban scheme used in the study that does not provide reliable estimates of ET (Fig. S2). ET is obtained as a sum of three components in Noah-MP that constitutes evaporation of canopy intercepted water (E_{CAN}), transpiration (E_{TRAN}), and soil surface evaporation (E_{DIR}). E_{CAN} and E_{TRAN} are dominated by the forest regions whereas croplands had higher E_{DIR} .

Fig. 3 shows the comparison between the modeled soil moisture (top 10 cm layer) and the observed SCAN soil moisture for five locations. The left panels show a temporal series of soil moisture from 2002 to 2008, the middle panels display the seasonal climatological cycle from 2002 to 2008, and the right panel shows the sites georeferenced in the study area. As indicated in Fig. 3, all model predictions show $R^2 > 0.6$ and $RMSE < 0.1$, but the model tends to have a much more damped response than observed. The top 10 cm soil moisture layer was highly sensitive to the seasonality of precipitation and its partitioning. Indeed, Cai et al. (2014a) showed similar

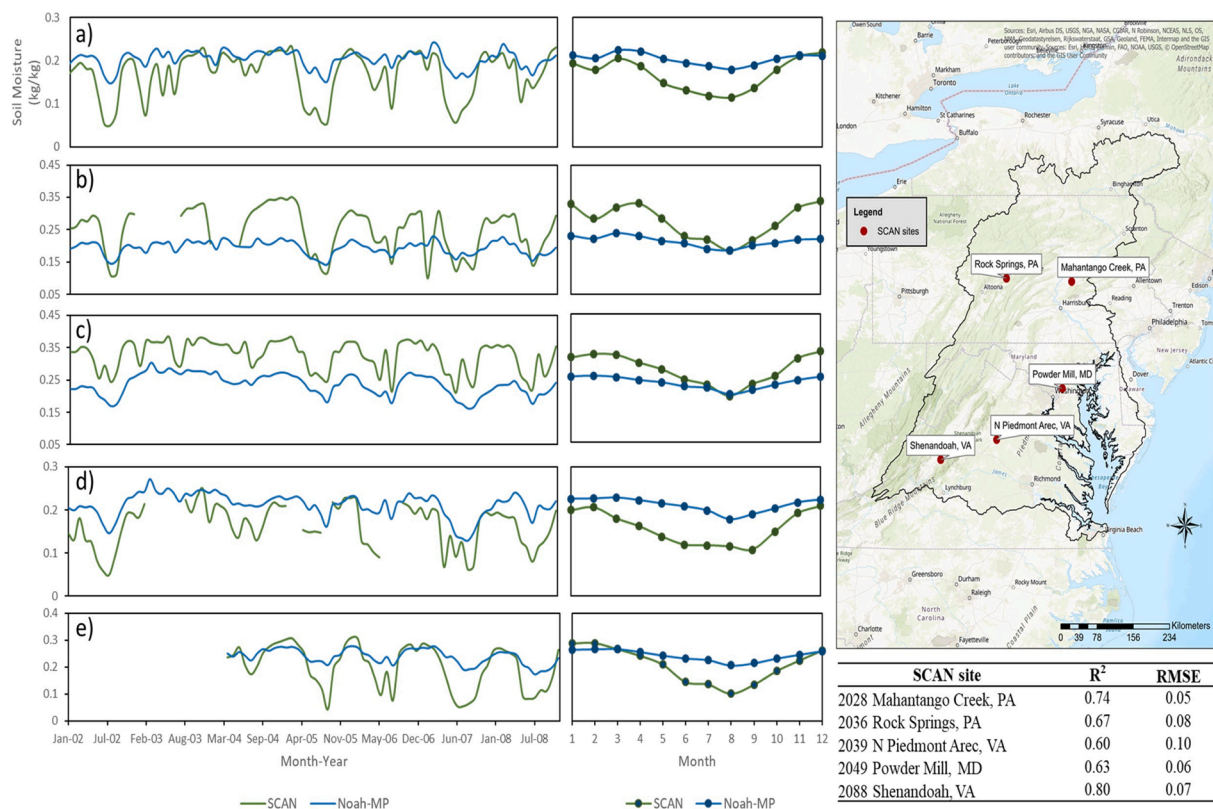


Fig. 3. Temporal series of soil moisture (left; 2002–2008) and the seasonal climatological cycle of soil moisture (right; 2002–2008) at five locations – a) Mahantango Creek, PA; b) Rock Springs, PA; c) N Piedmont Arec, VA d) Powder Mill, MD, and e) Shenandoah, VA. The statistics are displayed in the table on the bottom right.

soil moisture predictions in the Northeast region, a damped response to drying and wetting conditions. However, (Cai et al., 2014b; Yang et al., 2011; Zhuo et al., 2019) all showed much better model predictions of soil moisture when conditions were less variable. The uncertainty in model output was also introduced due to underlying assumptions of the Noah-MP land surface parameterization schemes. For example, the use of SIMTOP as a runoff scheme tends to retain more water in the soil column (Yang et al., 2011).

4.2. Changes in terrestrial hydrology

Fig. 4 (a & b) shows the average monthly change and inter-model variation in the precipitation (%), and 2 m air temperature [K] respectively across the six selected GCMs. Fig. 4 (a) depicts the monthly precipitation change and inter-model variation. Precipitation increased by 9 % and 10 % in RCP 4.5 and RCP 8.5 scenarios in the 2061–2090 period as compared to the historical period (1976–2005). Interestingly, a consistent increase of 7.5 % in precipitation was observed across all models for RCP 4.5 in the 2021–2050 period, whereas there was greater uncertainty of ± 20 mm/month among the RCP 8.5 model scenarios with an overall mean change of 6 % in the 2021–2050 period. A larger mean difference was observed during the winter and spring seasons while greater variation was observed during the summer and fall seasons for both RCP 4.5 and RCP 8.5. Likewise, a lower inter-model variation of ± 5 mm/month was observed during the historical period for the winter and spring seasons as compared to the higher inter-model variation during the future period for the summer and fall seasons. A consistent increase was observed in the Appalachian Plateau and Valley region across all GCM's and scenarios except in the RCP 8.5 scenario during the 2021–2050 period, which was due to a decrease in precipitation in Pennsylvania and the lower portion of the Chesapeake Bay watershed (Fig. S3).

As shown in Fig. 4 (b), an overall increase of 2.8 K and 4.5 K is observed in RCP 4.5 and RCP 8.5 scenarios, respectively for the 2061–2090 period. Similar to precipitation, higher inter-model variation ± 2 K was seen during the summer and fall for the RCP 8.5 scenario for the 2061–2090 period. The change in temperature was uniform throughout the Chesapeake Bay watershed for all the scenarios (Fig. S3). Fig. 4 (c & d) represents the annual change relative to the historical mean from 1976 to 2005 along with the Sen's slope (Theil-Sen's estimator) for each scenario across the six GCM's. Fig. 4 (c) illustrates the increasing trends for all precipitation scenarios except for RCP 4.5 that indicates the decreasing trend towards the end period with a Sen's slope value of -0.99. Fig. 4 (d) shows a consistent increase in temperature for both RCP 4.5 and RCP 8.5 with a similar Sen's slope of 0.06 for the 2021–2050 and 2061–2090. However, a plateau in precipitation was observed in the RCP 4.5 scenario towards the end period with a non-significant Sen's slope. Hawkins (2015) used CMIP3 and CMIP5 climate projections and concluded an overall increase of 1.9 %–5.4 % in annual air temperature and an increase between 5.2 % and 15.2 % in annual total precipitation in 2080–2099, similar to the results from this study.

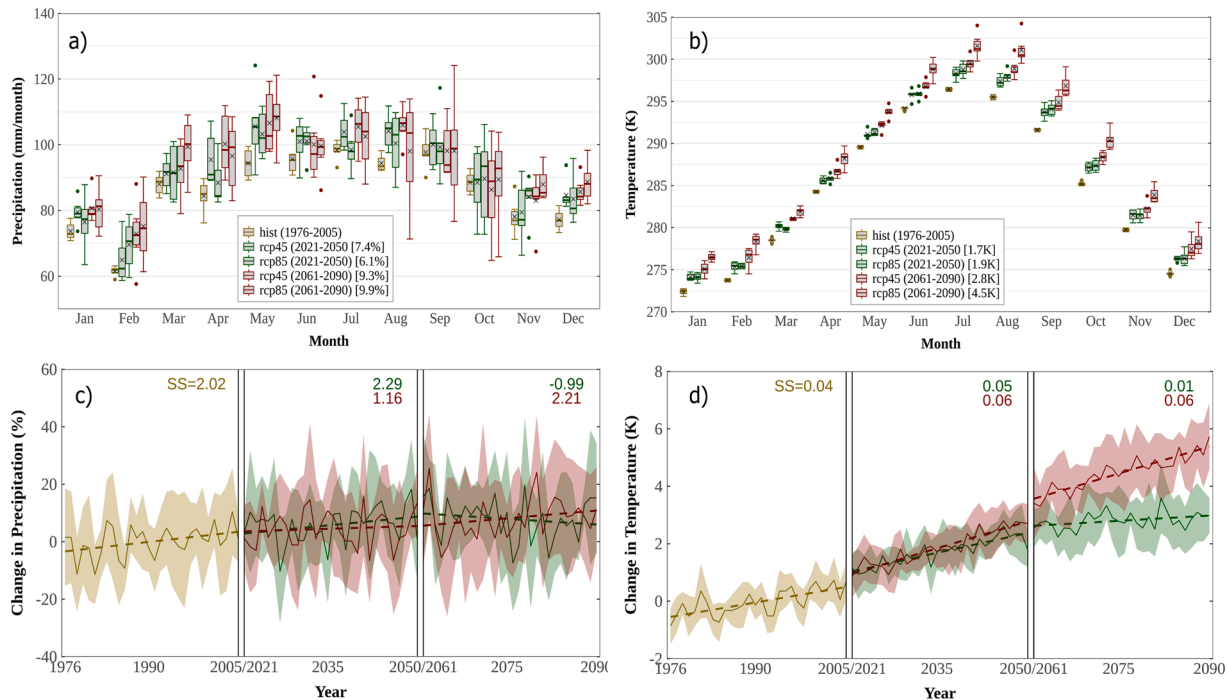


Fig. 4. Box plots (a & b) representing the climatological monthly uncertainty and change for historical and future scenarios for precipitation, and 2 m air temperature respectively for six GCM. The values in box brackets indicate an overall change with respect to the mean of historical data from 1976–2005 and 'x' denotes the mean. Plots (c & d) show the annual change (mean and one standard deviation as ribbon) for historical and future scenarios. The change is with respect to the mean of historical data from 1976–2005. The values colored indicate the Sen's slope (SS) for the respective scenarios. The units for SS are mm/yr, and K/yr for c and d respectively.

With increasing precipitation and rising temperatures, crop production and water availability are likely to be uncertain as it is dependent on multiple factors, including soil properties, crop type, the interaction between land surface processes, water management strategies, and atmospheric CO₂ levels. However, in regions with increasing temperatures and decreasing precipitation, soil water unavailability is often the limiting factor in crop production (Bhatt and Hossain, 2019).

4.3. Current and future crop water use (CW_U)

As described in section 3.7, daily crop coefficients, K_C , were calculated using the ratio of ETo from NOAA and actual ET from USGS SSEBop. The estimated ratios were averaged over the crop growth periods (Table S4) to derive the crop coefficients (Fig. 5). Fig. 5 (i–j) illustrates the daily crop coefficient curve for corn and soybeans with a 10-day moving mean. The corn [Fig. 5 (i)] and soybeans [Fig. 5

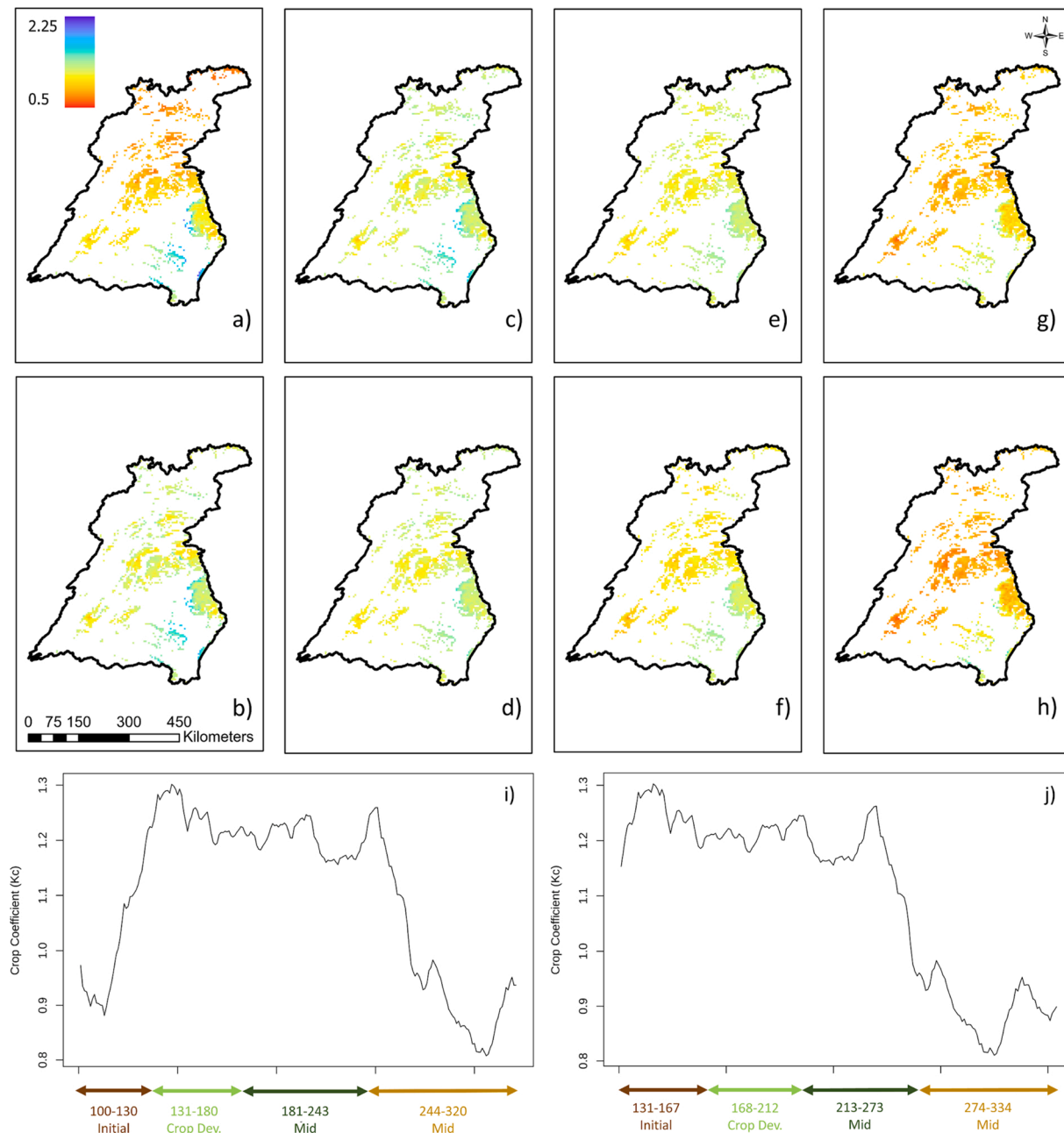


Fig. 5. Crop coefficients representing the average over Initial (a–b); Development (c–d); Middle (e–f) and Harvesting (g–h) period for corn and soybeans respectively. i and j shows daily crop coefficient for corn and soybeans respectively with a 10-day moving mean representing crop growth stages along with Julian day.

(j)] have similar K_C patterns but with different planting and harvesting dates. These K_C values were similar to the values determined by (Allen, 1998), who found average $K_{C[MID]}$ values of 1.15 for corn, and 1.20 for soybeans. The values for C_D approach 0.85 and 0.80 by 2100 for C_3 and C_4 crops, respectively. Further details on the temporal evolution of C_D for different RCP projections and crop species are described in Huntington et al. (2016).

The CW_U was calculated for both corn and soybeans by using the crop evapotranspiration and effective rainfall (Eq. 1), and an overall decline was observed in CW_U for both corn and soybeans. A decrease of 4 % and 13 % in CW_U is observed for corn under RCP 4.5 and RCP 8.5 scenario respectively, which is consistent with the decrease in the Sen's slope of -4 and -19 for the 2061–2090 period [Fig. 6(a–b)]. A similar trend is observed for soybeans indicating an overall decrease in CW_U of 6 % and 17 % in RCP 4.5 and RCP 8.5 scenarios for the 2061–2090 period, respectively [Fig. 6(c)]. The CW_U ranged from 50 mm/month during the initial crop growth phase to 100 mm/month during the peak crop growth phase.

Fig. 7 illustrates the different water balance components and the changes in crop evapotranspiration with and without the CO_2 correction factor. As shown in Fig. 7, the CW_U for both crops decreases due to an increase in the effective rainfall in both RCP 4.5 and RCP 8.5 scenarios resulting from the effect of increased CO_2 concentrations and increased total precipitation. Decreases in C_D values increase crop water use efficiency, resulting in reduced water consumption for both corn and soy crops in the Chesapeake Bay watershed. CW_U was more sensitive to the change in effective rainfall in the early growing period (Apr–May) due to an increase in precipitation whereas, in the mid growing period (Jun–Aug), lower evaporative demand caused a decrease in CW_U [Fig. 7 (b–e)]. The combined impact of increased precipitation and CO_2 emissions is responsible for a decrease in crop evapotranspiration and thereby the crop water use (Figs. 6 & 7). The impact of CO_2 levels in future scenarios is accounted for by the CO_2 correction factors, correcting transpiration in future periods. The stomatal conductance is suppressed by elevated CO_2 levels thereby decreasing the water loss and the evaporative flux.

This study estimated the change and uncertainty in CW_U using a combination of GCMs and a land surface model by accounting for complex land surface processes and factors including soil properties, crop type, climate variables, atmospheric CO_2 levels, and crop coefficients that determine the crop water use. The decrease in CW_U , assuming a fixed growing duration length and no change in cultivars, results in decreased crop evapotranspiration in agricultural areas in the Chesapeake Bay watershed. In summary, with an increase of 6–10 % in precipitation (Fig. 4) towards the end of the 21st century, a decrease of 13–17 % is estimated in CW_U (Fig. 6) primarily due to lower evaporative demand from increased photosynthetic efficiency. This is in contrast to many other regions, where climate change results in largely adverse effects on irrigated agriculture due to many concomitant changes (precipitation, temperature, ET, CO_2) acting on the system in complex and nonlinear ways (Nkomozepe and Chung, 2012; Yang et al., 2019).

Although this study used bias-corrected and downscaled GCM simulations to estimate change in CW_U , there exist uncertainties in intra-annual climate variability (Abatzoglou and Brown, 2012), and further resolving the timing of climate change impacts over the course of a growing season is critical (Mueller et al., 2015). CMIP Phase 6 is in development, and offers higher spatial resolution and

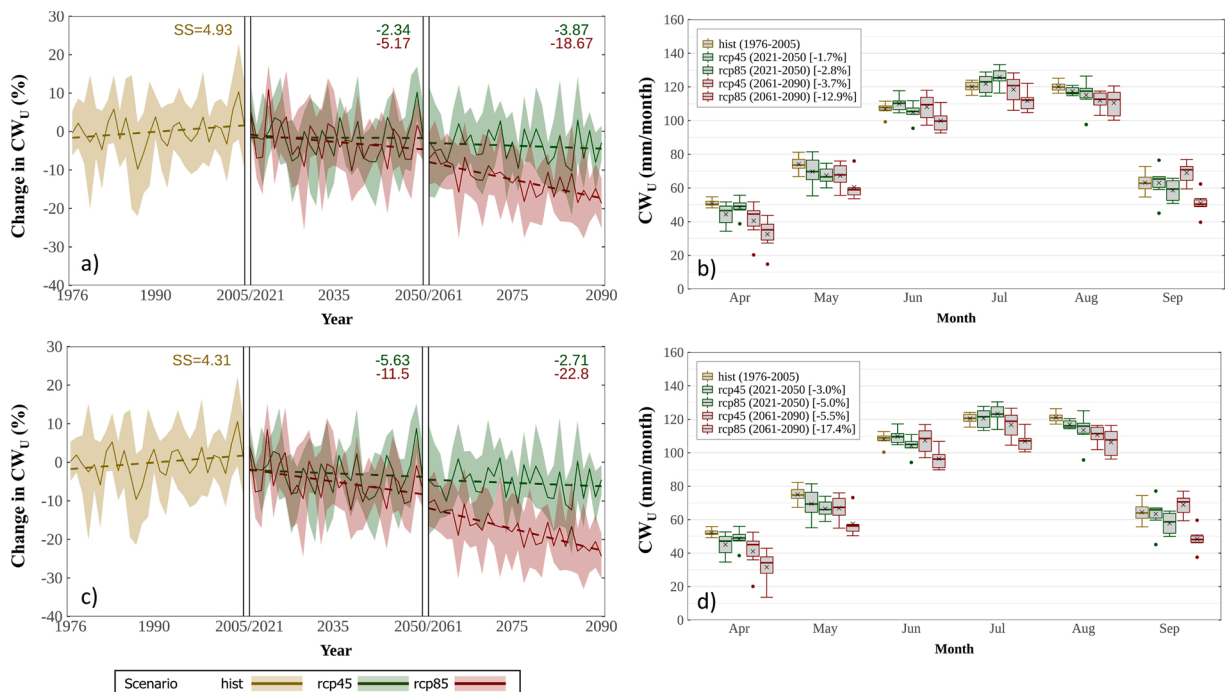


Fig. 6. Annual change (mean and one standard deviation, shading) in CW_U for corn and soybeans, respectively (a and c), indicate the Sen's slope for the respective scenarios. Boxplots (b and d) represent the monthly change and inter-model variation for crops and soybeans, respectively. Values in box brackets indicate the change relative to historical data (1976–2005). The SS unit for CW_U is $m^3/ha/yr$.

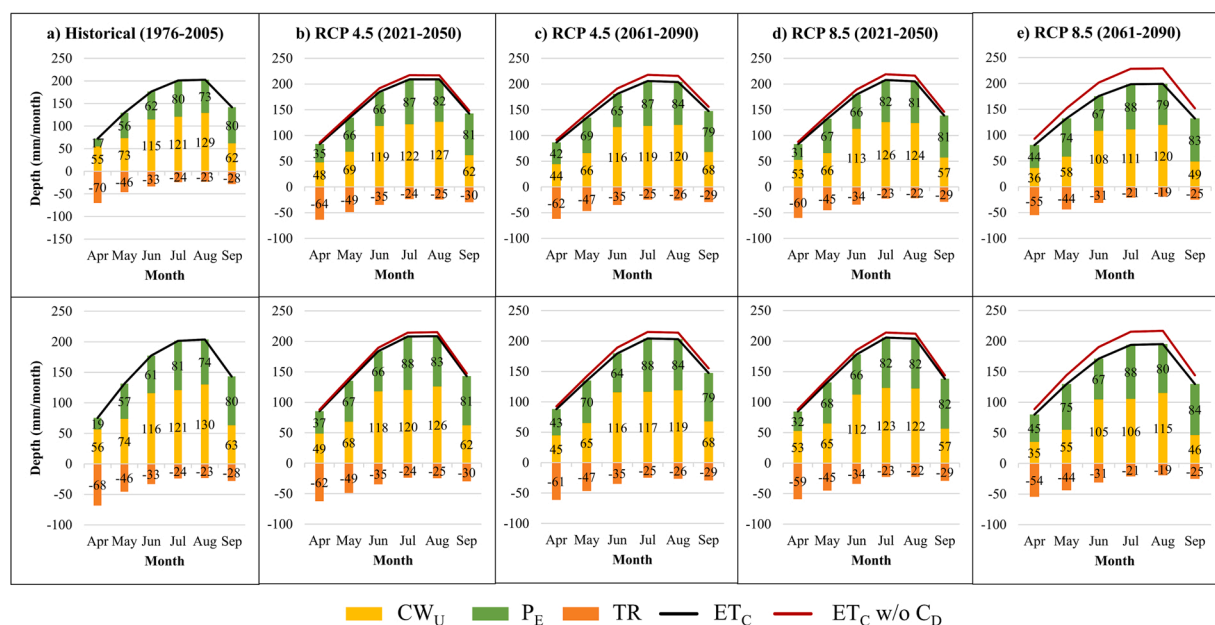


Fig. 7. Different water balance components illustrating the estimation of CW_U (Eq. 1). The top and bottom plots represent corn and soybeans, respectively for historical (a) and future scenarios (b-e).

The black and dark red line represents the crop evapotranspiration with and without CO_2 correction respectively.

better representation of processes (Eyring et al., 2016), but does not entirely resolve the intra-annual variability issue (Cook et al., 2020). Our results suggest that even a slight shift in the magnitude and timing of precipitation, for example, a 15 % decrease in winter/spring precipitation results in early growing season water stress, and can ultimately propagate through the entire growing season, impacting cumulative CW_U .

5. Conclusions

Noah-MP, in combination with GCM's, was used to assess the change in the terrestrial hydrological components across Chesapeake Bay agricultural lands, due to climate change and variability. CW_U is important to understand for future water resource use management, crop production potential, and developing mitigation strategies. Using available evapotranspiration products, daily crop coefficients for corn and soybeans are generated. The impacts of CO_2 levels on crop coefficients in future scenarios are accounted for by using the CO_2 correction factor considering the soybeans as C_3 and corn as C_4 crops. The soil water balance is then used to calculate the CW_U for the pixels dominated by corn and soybeans. The results suggest a significant increase in precipitation and temperature over the entire Chesapeake Bay watershed for both RCP 4.5 and RCP 8.5 scenarios in future periods, higher effective rainfall during the growing season, resulting from increased total precipitation and increased CO_2 concentrations, leads to a decrease of 13 % and 17 % in CW_U for corn and soybeans, respectively in the RCP 8.5 scenario for 2061–2090 as compared to 4 % and 6 % in the RCP 4.5 scenario. With the increasing availability of global datasets (remotely sensed, land-based station, and modeled) such as irrigation maps (Portmann et al., 2010; Siebert et al., 2015), high-resolution bias-corrected CMIP5 projections (Navarro-Racines et al., 2020) and reanalysis datasets [ERA5 (Hersbach et al., 2020); MERRA2 (Gelaro et al., 2017)], this approach can be scaled globally in data-scarce regions.

Data availability

The datasets generated or analyzed during the current study are available from (Modi et al., 2021).

Funding

This work was supported in part by the National Science Foundation (NSF), Water, Sustainability, and Climate Program (grant number CBET-1360280)

Author statement

Parthkumar A. Modi: Conceptualization; Formal analysis; Investigation; Methodology; Roles/Writing - original draft; Writing - review & editing

Daniel R. Fuka: Data curation; Methodology; Roles/Writing - original draft ; Software; Writing - review & editing

Zachary M. Easton: Conceptualization; Funding acquisition; Project administration; Roles/Writing - original draft; Writing - review & editing

Declaration of Competing Interest

The authors report no declarations of interest.

Appendix A. Supplementary data

Supplementary material related to this article can be found, in the online version, at doi:<https://doi.org/10.1016/j.ejrh.2021.100830>.

References

- Abatzoglou, J.T., 2013. Development of gridded surface meteorological data for ecological applications and modelling. *Int. J. Climatol.* 33, 121–131. <https://doi.org/10.1002/joc.3413>.
- Abatzoglou, J.T., Brown, T.J., 2012. A comparison of statistical downscaling methods suited for wildfire applications: statistical downscaling for Wildfire Applications. *Int. J. Climatol.* 32, 772–780. <https://doi.org/10.1002/joc.2312>.
- Allen, R.G. (Ed.), 1998. *Crop Evapotranspiration: Guidelines for Computing Crop Water Requirements*, FAO Irrigation and Drainage Paper. Food and Agriculture Organization of the United Nations, Rome.
- Baldini, L.M., Baldini, J.U.L., McElwaine, J.N., Frappier, A.B., Asmerom, Y., Liu, K., Pruger, K.M., Ridley, H.E., Polyak, V., Kennett, D.J., Macpherson, C.G., Aquino, V., Awe, J., Breitenbach, S.F.M., 2016. Persistent northward North Atlantic tropical cyclone track migration over the past five centuries. *Sci. Rep.* 6, 37522. <https://doi.org/10.1038/srep37522>.
- Bhatt, R., Hossain, A., 2019. Concept and consequence of evapotranspiration for sustainable crop production in the era of climate change. In: Bucur, D. (Ed.), *Advanced Evapotranspiration Methods and Applications*. IntechOpen. <https://doi.org/10.5772/intechopen.83707>.
- Brown, M.E., Antle, J.M., Backlund, P., Carr, E.R., Easterling, W.E., Walsh, M.K., Ammann, C., Attavanich, W., Barrett, C.B., Bellemare, M.F., Dancheck, V., Funk, C., Grace, K., Ingram, J.S.I., Jiang, H., Maletta, H., Mata, T., Murray, A., Ngugi, M., Ojima, D., O'Neill, B., Tebaldi, C., 2015. Climate change, global food security, and the U.S. Food system. U.S. Global Change Research Program. <https://doi.org/10.7930/J0862DC7>.
- Cai, X., Yang, Z.-L., David, C.H., Niu, G.-Y., Rodell, M., 2014a. Hydrological evaluation of the Noah-MP land surface model for the Mississippi River Basin. *J. Geophys. Res. Atmos.* 119, 23–38. <https://doi.org/10.1002/2013JD020792>.
- Cai, X., Yang, Z.-L., Xia, Y., Huang, M., Wei, H., Leung, L.R., Ek, M.B., 2014b. Assessment of simulated water balance from Noah, Noah-MP, CLM, and VIC over CONUS using the NLDAS test bed. *J. Geophys. Res. Atmos.* 119 (13) <https://doi.org/10.1002/2014JD022113>, 751–13,770.
- Chesapeake Bay Program, 2017. Facts & Figures | Chesapeake Bay Program [WWW Document]. URL <https://www.chesapeakebay.net/discover/facts> (accessed 7.27.20)..
- Cook, B.I., Mankin, J.S., Marvel, K., Williams, A.P., Smerdon, J.E., Anchukaitis, K.J., 2020. Twenty-first century drought projections in the CMIP6 forcing scenarios. *Earth's Future* 8. <https://doi.org/10.1029/2019EF001461>.
- Daly, C., Halbleib, M., Smith, J.I., Gibson, W.P., Doggett, M.K., Taylor, G.H., Curtis, J., Pasteris, P.P., 2008. Physiographically sensitive mapping of climatological temperature and precipitation across the conterminous United States. *Int. J. Climatol.* 28, 2031–2064. <https://doi.org/10.1002/joc.1688>.
- Deryng, D., Elliott, J., Folberth, C., Müller, C., Pugh, T.A.M., Boote, K.J., Conway, D., Ruane, A.C., Jones, J.W., Khabarov, N., Olin, S., Schaphoff, S., Schmid, E., Yang, H., Rosenzweig, C., 2016. Regional disparities in the beneficial effects of rising CO₂ concentrations on crop water productivity. *Nat. Clim. Change* 6, 786–790. <https://doi.org/10.1038/nclimate2995>.
- Döll, P., Siebert, S., 2002. Global modeling of irrigation water requirements: global modeling of irrigation water requirements. *Water Resour. Res.* 38, 8–1–8–10. <https://doi.org/10.1029/2001WR000355>.
- Ek, M.B., Mitchell, K.E., Lin, Y., Rogers, E., Grunmann, P., Koren, V., Gayno, G., Tarpley, J.D., 2003. Implementation of Noah land surface model advances in the National Centers for Environmental Prediction operational mesoscale Eta model. *J. Geophys. Res. Atmos.* 108 <https://doi.org/10.1029/2002JD003296>, 2002JD003296.
- Elliott, J., Deryng, D., Müller, C., Frieler, K., Konzmann, M., Gerten, D., Glotter, M., Flörke, M., Wada, Y., Best, N., Eisner, S., Fekete, B.M., Folberth, C., Foster, I., Gosling, S.N., Haddeland, I., Khabarov, N., Ludwig, F., Masaki, Y., Olin, S., Rosenzweig, C., Ruane, A.C., Satoh, Y., Schmid, E., Stacke, T., Tang, Q., Wisser, D., 2014. Constraints and potentials of future irrigation water availability on agricultural production under climate change. *Proc. Natl. Acad. Sci.* 111, 3239–3244. <https://doi.org/10.1073/pnas.1222474110>.
- Eyring, V., Bony, S., Meehl, G.A., Senior, C.A., Stevens, B., Stouffer, R.J., Taylor, K.E., 2016. Overview of the Coupled Model Intercomparison Project Phase 6 (CMIP6) experimental design and organization. *Geosci. Model. Dev. Discuss.* 9, 1937–1958. <https://doi.org/10.5194/gmd-9-1937-2016>.
- Fischer, G., Tubiello, F.N., van Velthuisen, H., Wiberg, D.A., 2007. Climate change impacts on irrigation water requirements: effects of mitigation, 1990–2080. *Technol. Forecast. Soc. Change* 74, 1083–1107. <https://doi.org/10.1016/j.techfore.2006.05.021>.
- Gelaro, R., McCarty, W., Suárez, M.J., Todling, R., Molod, A., Takacs, L., Randles, C.A., Darmenov, A., Bosilovich, M.G., Reichle, R., Wargan, K., Coy, L., Cullather, R., Draper, C., Akella, S., Buchard, V., Conaty, A., da Silva, A.M., Gu, W., Kim, G.-K., Koster, R., Lucchesi, R., Merkova, D., Nielsen, J.E., Partyka, G., Pawson, S., Putman, W., Rienecker, M., Schubert, S.D., Sienkiewicz, M., Zhao, B., 2017. The modern-era retrospective analysis for research and applications, version 2 (MERRA-2). *J. Clim.* 30, 5419–5454. <https://doi.org/10.1175/JCLI-D-16-0758.1>.
- Glotter, M., Elliott, J., McInerney, D., Best, N., Foster, I., Moyer, E.J., 2014. Evaluating the utility of dynamical downscaling in agricultural impacts projections. *Proc. Natl. Acad. Sci. U.S.A.* 111, 8776–8781. <https://doi.org/10.1073/pnas.1314787111>.
- Hagemann, S., Chen, C., Haerter, J.O., Heinke, J., Gerten, D., Piani, C., 2011. Impact of a statistical Bias correction on the projected hydrological changes obtained from three GCMs and two hydrology models. *J. Hydrometeorol.* 12, 556–578. <https://doi.org/10.1175/2011JHM1336.1>.
- Hawkins, T.W., 2015. Simulating the impacts of projected climate change on streamflow hydrology for the Chesapeake Bay Watershed. *Ann. Assoc. Am. Geogr.* 105, 627–648. <https://doi.org/10.1080/00045608.2015.1039108>.
- Hayhoe, K., Wake, C.P., Huntington, T.G., Luo, L., Schwartz, M.D., Sheffield, J., Wood, E., Anderson, B., Bradbury, J., DeGaetano, A., Troy, T.J., Wolfe, D., 2007. Past and future changes in climate and hydrological indicators in the US Northeast. *Clim. Dyn.* 28, 381–407. <https://doi.org/10.1007/s00382-006-0187-8>.
- He, L., Asseng, S., Zhao, G., Wu, D., Yang, X., Zhuang, W., Jin, N., Yu, Q., 2015. Impacts of recent climate warming, cultivar changes, and crop management on winter wheat phenology across the Loess Plateau of China. *Agric. For. Meteorol.* 200, 135–143. <https://doi.org/10.1016/j.agrformet.2014.09.011>.
- Hersbach, H., Bell, B., Berrisford, P., Hirahara, S., Horányi, A., Muñoz-Sabater, J., Nicolas, J., Peubey, C., Radu, R., Schepers, D., Simmons, A., Soci, C., Abdalla, S., Abellan, X., Balsamo, G., Bechtold, P., Biavati, G., Bidlot, J., Bonavita, M., Chiara, G., Dahlgren, P., Dee, D., Diamantakis, M., Dragani, R., Flemming, J., Forbes, R., Fuentes, M., Geer, A., Haimberger, L., Healy, S., Hogan, R.J., Hólm, E., Janisková, M., Keeley, S., Laloyaux, P., Lopez, P., Lupu, C., Radnoti, G.,

- Rosnay, P., Rozum, I., Vamborg, F., Villaume, S., Thépaut, J., 2020. The ERA5 global reanalysis. *Q. J. R. Meteorol. Soc.* 146, 1999–2049. <https://doi.org/10.1002/qj.3803>.
- Hidalgo, H.G., Dettinger, M.D., Cayan, D.R., 2008. Downscaling with constructed analogues: daily precipitation and temperature fields over the United States. *Calif. Clim. Change* 48, 62pp.
- Holzworth, D., Huth, N.I., Fainges, J., Brown, H., Zurcher, E., Cichota, R., Verrall, S., Herrmann, N.I., Zheng, B., Snow, V., 2018. APSIM Next Generation: overcoming challenges in modernising a farming systems model. *Environ. Model. Softw.* 103, 43–51. <https://doi.org/10.1016/j.envsoft.2018.02.002>.
- Huntington, J.L., Morton, C.G., Mcevoy, D., Bromley, M., Hedgewisch, K., Allen, R., Gangopadhyay, Subhrendu, 2016. Historical and Future Irrigation Water Requirements for Select Reclamation Project Areas, Western U.S. <https://doi.org/10.13140/RG.2.2.23078.93761>.
- Hurkmans, R.T.W.L., de Moel, H., Aerts, J.C.J.H., Troch, P.A., 2008. Water balance versus land surface model in the simulation of Rhine river discharges: water balance versus Land Surface Model. *Water Resour. Res.* 44 <https://doi.org/10.1029/2007WR006168>.
- Jacobs, C.M.J., Bruin, H.A.R.D., 1992. The sensitivity of regional transpiration to land-surface characteristics: significance of feedback. *J. Clim.* 5, 683–698. [https://doi.org/10.1175/1520-0442\(1992\)005<0683:TSORTT>2.0.CO;2](https://doi.org/10.1175/1520-0442(1992)005<0683:TSORTT>2.0.CO;2).
- Jacobs, C.M.J., Bruin, H.A.R.D., 1997. Predicting regional transpiration at elevated atmospheric CO₂: influence of the PBL–vegetation interaction. *J. Appl. Meteorol. Climatol.* 36, 1663–1675. [https://doi.org/10.1175/1520-0450\(1997\)036<1663:PRTAEA>2.0.CO;2](https://doi.org/10.1175/1520-0450(1997)036<1663:PRTAEA>2.0.CO;2).
- Kimball, Idso, 1983. Increasing atmospheric CO₂: effects on crop yield, water use and climate. *Agric. Water Manage.* [https://doi.org/10.1016/0378-3774\(83\)90075-6](https://doi.org/10.1016/0378-3774(83)90075-6).
- Koehler, A.-K., 2020. Uncertainties in global crop modelling. *Nat. Food* 1, 19–20. <https://doi.org/10.1038/s43016-019-0008-y>.
- Konzmann, M., Gerten, D., Heinke, J., 2013. Climate impacts on global irrigation requirements under 19 GCMs, simulated with a vegetation and hydrology model. *Hydrol. Sci. J.* 58, 88–105. <https://doi.org/10.1080/02626667.2013.746495>.
- Kruijft, B., Witte, J.-P.M., Jacobs, C.M.J., Kroon, T., 2008. Effects of rising atmospheric CO₂ on evapotranspiration and soil moisture: a practical approach for the Netherlands. *J. Hydrol.* 349, 257–267. <https://doi.org/10.1016/j.jhydrol.2007.10.052>.
- Lehner, B., Verdin, K., Jarvis, A., 2008. New global hydrography derived from spaceborne elevation data. *Eos Trans. Am. Geophys. Union* 89, 93. <https://doi.org/10.1029/2008EO100001>.
- Liu, Y., Wang, E., Yang, X., Wang, J., 2009. Contributions of climatic and crop varietal changes to crop production in the North China Plain, since 1980s: Crop yield impacted by crop variety and climate. *Glob. Change Biol.* 16, 2287–2299. <https://doi.org/10.1111/j.1365-2486.2009.02077.x>.
- Liu, L., Wang, E., Zhu, Y., Tang, L., 2012. Contrasting effects of warming and autonomous breeding on single-rice productivity in China. *Agric. Ecosyst. Environ.* 149, 20–29. <https://doi.org/10.1016/j.agee.2011.12.008>.
- Lohmann, D., Nolte-Holube, R., Raschke, E., 1996. A large-scale horizontal routing model to be coupled to land surface parametrization schemes. *Tellus A* 48, 708–721. <https://doi.org/10.1034/j.1600-0870.1996.t013-0-00009.x>.
- Maloney, E.D., Camargo, S.J., Chang, E., Colle, B., Fu, R., Geil, K.L., Hu, Q., Jiang, X., Johnson, N., Karnauskas, K.B., Kinter, J., Kirtman, B., Kumar, S., Langenbrunner, B., Lombardo, K., Long, L.N., Mariotti, A., Meyerson, J.E., Mo, K.C., Neelin, J.D., Pan, Z., Seager, R., Serra, Y., Seth, A., Sheffield, J., Stroeve, J., Thibeault, J., Xie, S.-P., Wang, C., Wyman, B., Zhao, M., 2014. North american climate in CMIP5 experiments: part III: assessment of twenty-first-century projections*. *J. Clim.* 27, 2230–2270. <https://doi.org/10.1175/JCLI-D-13-00273.1>.
- Maurer, E.P., Hidalgo, H.G., Das, T., Dettinger, M.D., Cayan, D.R., 2010. The utility of daily large-scale climate data in the assessment of climate change impacts on daily streamflow in California. *Hydrol. Earth Syst. Sci.* 14, 1125–1138. <https://doi.org/10.5194/hess-14-1125-2010>.
- Mishra, V., Kumar, D., Ganguly, A.R., Sanjay, J., Mujumdar, M., Krishnan, R., Shah, R.D., 2014. Reliability of regional and global climate models to simulate precipitation extremes over India. *J. Geophys. Res. Atmospheres* 119, 9301–9323. <https://doi.org/10.1002/2014JD021636>.
- Mitchell, K.E., 2004. The multi-institution North American Land Data Assimilation System (NLDAS): utilizing multiple GCIP products and partners in a continental distributed hydrological modeling system. *J. Geophys. Res.* 109, D07S90 <https://doi.org/10.1029/2003JD003823>.
- Modi, P., Easton, Z., Fuka, D.R., 2021. Data in Support of the Manuscript “Impacts of Climate Change on Terrestrial Hydrological Components and Crop Water Requirement in the Chesapeake Bay Watershed.” <https://doi.org/10.6084/M9.FIGSHARE.14049569>.
- Mueller, B., Hauser, M., Iles, C., Rimi, R.H., Zwiers, F.W., Wan, H., 2015. Lengthening of the growing season in wheat and maize producing regions. *Weather Clim. Extrem.* 9, 47–56. <https://doi.org/10.1016/j.wace.2015.04.001>.
- Najjar, R.G., Pyke, C.R., Adams, M.B., Breitburg, D., Hershner, C., Kemp, M., Howarth, R., Mulholland, M.R., Paolisso, M., Secor, D., Sellner, K., Wardrop, D., Wood, R., 2010. Potential climate-change impacts on the Chesapeake Bay. *Estuar. Coast. Shelf Sci.* 86, 1–20. <https://doi.org/10.1016/j.ecss.2009.09.026>.
- National Engineering Handbook, 1993. National resources conservation service. *National engineering handbook*, part 623. Chapter 2. In: Martin, Derrel L., Gilly, James R. (Eds.), *Irrigation Water Requirements* (210-vi-NEH), 304.
- Navarro-Racines, C., Tarapues, J., Thornton, P., Jarvis, A., Ramirez-Villegas, J., 2020. High-resolution and bias-corrected CMIP5 projections for climate change impact assessments. *Sci. Data* 7, 7. <https://doi.org/10.1038/s41597-019-0343-8>.
- Niu, G.-Y., Yang, Z.-L., Dickinson, R.E., Gulden, L.E., 2005. A simple TOPMODEL-based runoff parameterization (SIMPOT) for use in global climate models. *J. Geophys. Res.* 110, D21106 <https://doi.org/10.1029/2005JD006111>.
- Niu, G.-Y., Yang, Z.-L., Dickinson, R.E., Gulden, L.E., Su, H., 2007. Development of a simple groundwater model for use in climate models and evaluation with Gravity Recovery and Climate Experiment data. *J. Geophys. Res.* 112, D07103 <https://doi.org/10.1029/2006JD007522>.
- Niu, G.-Y., Yang, Z.-L., Mitchell, K.E., Chen, F., Ek, M.B., Barlage, M., Kumar, A., Manning, K., Niyogi, D., Rosero, E., Tewari, M., Xia, Y., 2011. The community Noah land surface model with multiparameterization options (Noah-MP): 1. Model description and evaluation with local-scale measurements. *J. Geophys. Res.* 116, D12109 <https://doi.org/10.1029/2010JD015139>.
- Nkomozepi, Temba, Chung, 2012. Assessing the trends and uncertainty of maize net irrigation water requirement estimated from climate change projections for Zimbabwe. *Agric. Water Manage.* <https://doi.org/10.1016/j.agwat.2012.05.004>.
- Portmann, F.T., Siebert, S., Döll, P., 2010. MIRCA2000-Global monthly irrigated and rainfed crop areas around the year 2000: a new high-resolution data set for agricultural and hydrological modeling: MONTHLY IRRIGATED AND RAINFED CROP AREAS. *Glob. Biogeochem. Cycles* 24. <https://doi.org/10.1029/2008GB003435> n/a-n/a.
- Pyke, C.R., Najjar, R.G., Adams, M.B., Breitburg, D., Kemp, M., Hershner, C., Howarth, R., Mulholland, M.R., Paolisso, M., Secor, D., Sellner, K., Wardrop, D., Wood, R., 2008. Climate Change and the Chesapeake Bay: State-of-the-Science Review and Recommendations. A Report from the Chesapeake Bay Program Science and Technical Advisory Committee (STAC), Annapolis, MD, 59pp.
- Reichler, T., Kim, J., 2008. How well do coupled models simulate today's climate? *Bull. Am. Meteorol. Soc.* 89, 303–312. <https://doi.org/10.1175/BAMS-89-3-303>.
- Rosenzweig, C., Strzepek, K.M., Major, D.C., Iglesias, A., Yates, D.N., McCluskey, A., Hillel, D., 2004. Water resources for agriculture in a changing climate: international case studies. *Glob. Environ. Change* 14, 345–360. <https://doi.org/10.1016/j.gloenvcha.2004.09.003>.
- Sacks, W.J., Kucharik, C.J., 2011. Crop management and phenology trends in the U.S. Corn Belt: impacts on yields, evapotranspiration and energy balance. *Agric. For. Meteorol.* 151, 882–894. <https://doi.org/10.1016/j.agrformet.2011.02.010>.
- Schaake, J.C., Koren, V.I., Duan, Q.-Y., Mitchell, K., Chen, F., 1996. Simple water balance model for estimating runoff at different spatial and temporal scales. *J. Geophys. Res. Atmospheres* 101, 7461–7475. <https://doi.org/10.1029/95JD02892>.
- Schaefer, G.L., Cosh, M.H., Jackson, T.J., 2007. The USDA natural resources conservation service soil climate analysis network (SCAN). *J. Atmospheric Ocean. Technol.* 24, 2073–2077. <https://doi.org/10.1175/2007JTECHA930.1>.
- Sen, P.K., 1968. Estimates of the regression coefficient based on Kendall's tau. *J. Am. Stat. Assoc.* 63, 1379–1389. <https://doi.org/10.1080/01621459.1968.10480934>.
- Senay, G.B., Verdin, J.P., Lietzow, R., Melesse, A.M., 2008. Global daily reference evapotranspiration modeling and evaluation ¹. *JAWRA J. Am. Water Resour. Assoc.* 44, 969–979. <https://doi.org/10.1111/j.1752-1688.2008.00195.x>.
- Senay, G.B., Bohms, S., Singh, R.K., Gowda, P.H., Velpuri, N.M., Alemu, H., Verdin, J.P., 2013. Operational evapotranspiration mapping using remote sensing and weather datasets: a new parameterization for the SSEB approach. *JAWRA J. Am. Water Resour. Assoc.* 49, 577–591. <https://doi.org/10.1111/jawr.12057>.

- Sheffield, J., Barrett, A.P., Colle, B., Nelun Fernando, D., Fu, R., Geil, K.L., Hu, Q., Kinter, J., Kumar, S., Langenbrunner, B., Lombardo, K., Long, L.N., Maloney, E., Mariotti, A., Meyerson, J.E., Mo, K.C., David Neelin, J., Nigam, S., Pan, Z., Ren, T., Ruiz-Barradas, A., Serra, Y.L., Seth, A., Thibeault, J.M., Stroeve, J.C., Yang, Z., Yin, L., 2013. North American Climate in CMIP5 Experiments. Part I: Evaluation of Historical Simulations of Continental and Regional Climatology. *J. Clim.* 26, 9209–9245. <https://doi.org/10.1175/JCLI-D-12-00592.1>.
- Siebert, S., Kumm, M., Porkka, M., Döll, P., Ramankutty, N., Scanlon, B.R., 2015. A global data set of the extent of irrigated land from 1900 to 2005. *Hydrol. Earth Syst. Sci.* 19, 1521–1545. <https://doi.org/10.5194/hess-19-1521-2015>.
- Solomon, S., Intergovernmental Panel on Climate Change, Intergovernmental Panel on Climate Change (Eds.), 2007. *Climate Change 2007: the Physical Science Basis: Contribution of Working Group I to the Fourth Assessment Report of the Intergovernmental Panel on Climate Change*. Cambridge University Press, Cambridge, New York.
- Solomon, S., Plattner, G.-K., Knutti, R., Friedlingstein, P., 2009. Irreversible climate change due to carbon dioxide emissions. *Proc. Natl. Acad. Sci.* 106, 1704–1709. <https://doi.org/10.1073/pnas.0812721106>.
- Stöckle, C.O., Kemanian, A.R., 2020. Can crop models identify critical gaps in genetics, environment, and management interactions? *Front. Plant Sci.* 11, 737. <https://doi.org/10.3389/fpls.2020.00737>.
- Strahler, A., Muchoney, D., Borak, J., Friedl, M., Gopal, S., Lambin, E., Moody, A., 1999. MODIS Land Cover and Land-Cover Change 72.
- Sun, L., Anderson, M.C., Gao, F., Hain, C., Alfieri, J.G., Sharifi, A., McCarty, G.W., Yang, Yun, Yang, Yang, KUSTAS, W.P., McKee, L., 2017. Investigating water use over the choptank river watershed using a multisatellite data fusion approach: WATER USE OVER THE CHOPTANK WATERSHED. *Water Resour. Res.* 53, 5298–5319. <https://doi.org/10.1002/2017WR020700>.
- Taylor, K.E., Stouffer, R.J., Meehl, G.A., 2012. An overview of CMIP5 and the experiment design. *Bull. Am. Meteorol. Soc.* 93, 485–498. <https://doi.org/10.1175/BAMS-D-11-00094.1>.
- Theil, H., 1950. A rank invariant method of linear and polynomial regression analysis, i, ii, iii. *Proc. K. Ned. Akad. Wet. Ser. Math. Sci.* 53, 386–392, 521–525, 1397–1412.
- UCAR/NCAR, 2020. WRF Preprocessing System (WPS) Geographical Static Data [WWW Document]. URL https://www2.mmm.ucar.edu/wrf/users/download/get_sources_wps_geog.html (accessed 7.27.19).
- Urban, D.W., Sheffield, J., Lobell, D.B., 2017. Historical effects of CO₂ and climate trends on global crop water demand. *Nat. Clim. Change* 7, 901–905. <https://doi.org/10.1038/s41558-017-0011-y>.
- USDA, 2008. CropScape - NASS CDL Program [WWW Document]. URL <https://nassgeodata.gmu.edu/CropScape/> (accessed 12.15.19).
- USDA-NASS, 2010. Field crops usual planting and harvesting dates 10/29/2010. *Agric. Handb. Number 628*, 51.
- van den Dool, H., 2003. Performance and analysis of the constructed analogue method applied to U.S. Soil moisture over 1981–2001. *J. Geophys. Res.* 108, 8617. <https://doi.org/10.1029/2002JD003114>.
- Van Den Dool, H.M., 1994. Searching for analogues, how long must we wait? *Tellus A* 46, 314–324. <https://doi.org/10.1034/j.1600-0870.1994.t01-2-00006.x>.
- Vanuytrecht, et al., 2012. Quantifying field-scale effects of elevated carbon dioxide concentration on crops. *Climate Research*. <https://doi.org/10.3354/cr01096>.
- Varanasi, A., Prasad, P.V.V., Jugulam, M., 2016. Impact of climate change factors on weeds and herbicide efficacy. *Advances in Agronomy*. Elsevier, pp. 107–146. <https://doi.org/10.1016/b.s.agron.2015.09.002>.
- Wagena, M.B., Easton, Z.M., 2018. Agricultural conservation practices can help mitigate the impact of climate change. *Sci. Total Environ.* 635, 132–143. <https://doi.org/10.1016/j.scitotenv.2018.04.110>.
- Wagena, M.B., Sommerlot, A., Abiy, A.Z., Collick, A.S., Langan, S., Fuka, D.R., Easton, Z.M., 2016. Climate change in the Blue Nile Basin Ethiopia: implications for water resources and sediment transport. *Clim. Change* 139, 229–243. <https://doi.org/10.1007/s10584-016-1785-z>.
- Wagena, M.B., Collick, A.S., Ross, A.C., Najjar, R.G., Rau, B., Sommerlot, A.R., Fuka, D.R., Kleinman, P.J.A., Easton, Z.M., 2018. Impact of climate change and climate anomalies on hydrologic and biogeochemical processes in an agricultural catchment of the Chesapeake Bay watershed. *USA. Sci. Total Environ* 637–638, 1443–1454. <https://doi.org/10.1016/j.scitotenv.2018.05.116>.
- Xia, Y., Mitchell, K., Ek, M., Cosgrove, B., Sheffield, J., Luo, L., Alonge, C., Wei, H., Meng, J., Livneh, B., Duan, Q., Lohmann, D., 2012. Continental-scale water and energy flux analysis and validation for North American Land Data Assimilation System project phase 2 (NLDAS-2): 2. Validation of model-simulated streamflow: VALIDATION OF MODEL-SIMULATED STREAMFLOW. *J. Geophys. Res. Atmos.* 117. <https://doi.org/10.1029/2011JD016051> n/a-n/a.
- Yang, Z.-L., Niu, G.-Y., Mitchell, K.E., Chen, F., Ek, M.B., Barlage, M., Longuevergne, L., Manning, K., Niyogi, D., Tewari, M., Xia, Y., 2011. The community Noah land surface model with multiparameterization options (Noah-MP): 2. Evaluation over global river basins. *J. Geophys. Res.* 116, D12110. <https://doi.org/10.1029/2010JD015140>.
- Yang, J., Ren, W., Ouyang, Y., Feng, G., Tao, B., Granger, J.J., Poudel, K.P., 2019. Projection of 21st century irrigation water requirement across the Lower Mississippi Alluvial Valley. *Agric. Water Manag.* 217, 60–72. <https://doi.org/10.1016/j.agwat.2019.02.033>.
- Zhang, T., Huang, Y., Yang, X., 2013. Climate warming over the past three decades has shortened rice growth duration in China and cultivar shifts have further accelerated the process for late rice. *Glob. Change Biol.* 19, 563–570. <https://doi.org/10.1111/gcb.12057>.
- Zhuo, L., Dai, Q., Han, D., Chen, N., Zhao, B., 2019. Assessment of simulated soil moisture from WRF Noah, Noah-MP, and CLM land surface schemes for landslide hazard application. *Hydrol. Earth Syst. Sci.* 23, 4199–4218. <https://doi.org/10.5194/hess-23-4199-2019>.